Precise Se-flux control and its effect on $Cu(In,Ga)Se_2$ absorber layer deposited at low substrate temperature by multi stage co-evaporation

Authors: Shiro Nishiwaki, Thomas Feurer, Benjamin Bissig, Enrico Avancini, Romain Carron, Stephan Buecheler, and Ayodhya N. Tiwari

Laboratory for Thin Films and Photovoltaics, Empa - Swiss Federal Laboratories for Materials Science and Technology, Ueberlandstrasse 129, 8600 Duebendorf, Switzerland

Abstract

In-situ Se flux control system is applied for the growth of $Cu(In,Ga)Se_2$ (CIGS) absorber layers by a multi stage thermal co-deposition of elements at low substrate temperature below 500 °C. It was revealed that the composition depth profile of the [Ga]/([In]+[Ga]) (GGI) ratio is affected by the [Se]/[Metal] flux ratio. It was observed for the solar cell properties that the change in the depth profiles of GGI induced by the change of [Se]/[Metal] resulted in an increase in the J_{SC} and a decrease in the FF, and hence little influence on the efficiency. Under control of [Se]/[Metal] ratio during the deposition process, the effect of CIGS layer thickness on the solar cell properties was investigated. With increase in the thickness up to 2.8 μm, the short circuit current density was increased to over 35 mA/cm^2 w/o AR coating, resulting in conversion efficiency above 18 % using low temperature deposition method.

1. Introduction

Recently, $Cu(In,Ga)Se_2$ (CIGS) thin film solar cells with efficiency of over 22 % were reported [1,2]. To achieve high solar cell efficiency, carful control of Se supply during the CIGS process is mandatory for layers grown by thermal co-evaporation of elements in vacuum. There are many reports on the effect - not only of the ratio of Se flux to the other metals - but also of the activity of Se during the deposition on the properties of CIGS solar cells [3–10]. However, the measurement of the flux of Se in a repetitive and quantitative manner during the process has always been an issue. Furthermore, this problem could be critical for large scale production, for example in a roll-to-roll production line, since assuring long term process stability without in situ monitoring is almost impossible.

Precise control of Se flux was realized by the combination of in-situ monitoring of optical absorption of UV light by Se vapor and a valved Se source in our previous work [11]. The effects of Se flux on the surface texture and the crystal orientation are reported for 3-stage deposition process at high substrate temperature and they are closely related to the conditions during the first stage of the evaporation process [4,9]. It is also reported that the solar cell properties deteriorate under low Se flux condition below [Se]/[Metal]=4 [6,9]. However, the substrate temperature during deposition should play an important role since it affects the chemical activity of Se. In this work, the Se flux controlling system is applied for the multi stage co-evaporation at low substrate temperature below 500 °C [12]. The effects of Se flux during the

growth of CIGS layers, especially during the 2nd stage, on the microstructure, composition depth profile, and device properties are discussed.

2. Experiments

CIGS absorber layers were deposited by a multi stage evaporation process at substrate temperature below 500 °C on Mo coated soda-lime glasses (DC sputtering). Subsequently, sodium fluoride post deposition treatment was applied on CIGS layer during cool-down of the substrate. This process is directly compatible with flexible polyimide substrates. Figure 1 shows typical relative fluxes of elements and substrate temperature during the CIGS growth process. The flux of Cu during growth was calculated from the chemical composition and thickness of final CIGS layers after the deposition process. The fluxes of In and Ga were determined by measuring the deposition rates on Mo coated soda-lime glasses substrates at well below 100 °C. For Se flux, since the UV light absorbance and the effusion rate is linearly correlated [11], the deposition rate on Mo coated soda-lime glass substrate at well below 100 °C was used to calibrate the flux during the CIGS deposition processes. During the deposition process, Se flux was precisely controlled by a flux monitoring system discussed elsewhere [11]. For this multi stage co-evaporation process, Se flux was kept constant through one run, so that [Se]/[Metal] ratio changes for individual stages. In the 1st stage [Se]/[Metal] ([Se]/([In]+[Ga])) was altered within the range of 3.3-10. It corresponds to the range of 2.5-7.5 in the 2nd stage and to the range of 10-30 in the 3rd stage. To characterize the rate of Se flux, the parameter of [Se]/[Metal] in the 2nd stage, which means [Se]/([Cu]+[Ga]), is used. In order to change the

thickness of CIGS layers, the deposition rates of metals were adjusted keeping the total deposition time. It should be noted that the relative flux rates between Cu, In, and Ga were kept almost constant in this work and the uncertainty of flux ratios could be ±20% at least. Concerning sodium fluoride post deposition treatment, regardless of the CIGS deposition processes, the same condition was adapted for all preparations and it was confirmed to be appropriate.

In order to characterize the CIGS layers, the chemical composition was determined by X-ray *fluorescence* (XRF, in house, *Rh target at 45 kV*), composition depth profiles of CIGS layers were analyzed by Time-of-flight secondary ions spectrometry (ION-TOF GmbH TOF.SIMS[5]) *with O_2^+ for sputtering and Bi^+ for analyzing*, and the microstructure of absorber layers were observed by scanning electron microscopy (SEM, Hitachi S-4800) *with an accelerating voltage of 5kV*. To investigate the solar cell properties, devices with a structure of Soda-lime glass/Mo/CIGS/CdS/i-ZnO/ZnO:Al/Ni-Al were processed. The CdS layer was grown by chemical bath deposition, the ZnO layers were deposited by RF sputtering, and the Ni-Al grid was deposited by e-beam evaporation. The solar cell properties were analyzed by measurements of external quantum efficiency (EQE) and current density-voltage curves.

3. Results and discussion

3.1. Effects of Se flux on the deposition process and the microstructure

CIGS layers were grown under various Se flux conditions keeping the chemical composition and thickness. The typical composition of CIGS layers through this work is [Cu]:[In]:[Ga]:[Se]=22.2:15.7:10.6:51.5 ([Cu]/([In]+[Ga])=0.847, [Ga]/([In]+[Ga])=0.402) and the thickness of CIGS layers used to evaluate the effect of Se flux is about 2.3 μm. It should be mentioned that within those experimental conditions in this work notable composition and thickness changes by re-evaporation reported [13,14] were not observed. The same as 3-stage deposition process [15], which is widely used for the growth of CIGS layers, in-situ [Cu]/([In]+[Ga]) composition monitoring as describ1ed in ref. [16] is applied also in the multi stage deposition process. Figure 2 shows power requirements to keep the substrate temperature constant during 2nd stage for typical and low [Se]/([Cu]+[Ga]) ratios. The arrowed positions correspond to the stoichiometry point calculated from the final film composition. As shown in Fig. 2, a clear increase in the power requirement is seen for typical Se flux at this point. This signal feature is known as the indication for the formation of Cu-Se phase at the surface of the growing CIGS layer during the 2nd stage of the 3-stage deposition process [16]. An essential of this relative composition detection method is that the Cu-Se phase is not formed until reaching [Cu]/([In]+[Ga])=1 under a preferred Se flux condition for high quality CIGS layers by the 3-stage deposition process. In contrast, under low Se flux condition no clear indication is seen, but slow increase in power output starting far before the stoichiometry point is measured as shown in Fig. 2. This type of response, related to lack of Se condition, is reported to be not preferable, and considered to originate

from the formation of second phases, such as Cu-Se phase [5]. Within our experiments, it was difficult to observe clear stoichiometry point for the flux ratios of [Se]/([Cu]+[Ga]) below 3.3. It should be mentioned that the sharp increase of power output at the right hand side of stoichiometry point shown in Fig. 2 results from the end of Cu deposition by a shutter at the end of 2nd stage.

Cross-section SEM images of CIGS layers grown under different Se flux conditions are shown in Fig. 3. The CIGS layer grown under low Se condition includes many voids (Fig. 3(a)). The CIGS layers grown with middle and high Se flux conditions show dense and similar grain structures (Fig. 3(b) and (c)). That difference in the microstructure suggests the change in the grain growth process during layers deposition.

Figure 4 presents the [Ga]/([Ga]+[In]) (GGI) composition depth profiles of CIGS layers prepared under low and high Se conditions, corresponding to the layers shown in Fig. 3. Clear difference of the profiles is observed in Fig. 4. The dependence of GGI depth grading on [Se]/[Metal] was not reported in previous works [6,9] and we think this is one of the characteristic of the multi stage process at low substrate temperature. The GGI composition grading from back contact to its minimum is mainly constructed during the 2nd stage of the growth process [17]. The formation of the grading depends on the chemistry of the chalcopyrite phase formation reaction at the growing film surface induced by the Cu deposition on Cu-poor Cu-(In,Ga)-Se layer, the slower diffusivity of Ga than In, and the concentration of Cu near the surface [18]. This suggests that the [Se]/[Metal] ratio affects the reaction chemistry and kinetics at the growing surface during the 2nd stage of the multi stage

evaporation process. Although the detail of the chemistry behind the observations is still unclear, one of the possible scenarios to explain the change in GGI profile in a manner consistent with Fig. 2 though Fig. 4 could be as follows;

1. Low [Se]/[Metal] condition increases Cu concentration at film surface.

2. The increased Cu concentration at surface results in early precipitation of Cu-Se phase Se, which relates with unclear endpoint detection and voids observed in microstructure.

3. The increased Cu concentration at the surface induces lowering of diffusivity of Ga also, which results in steep grading of the GGI [18,19].

3.2. Effects of Se flux on solar cell properties

Figure 5 shows solar cell parameters of devices with CIGS layers grown under various [Se]/[Metal] conditions. Closed circles show an average of small cells on one substrate (18 cells × ~0.57 cm^2), and the error bars indicate maximum and minimum results. Different from previous works [6,9], no significant deterioration of the solar cell performances with decreasing [Se]/[Metal] was observed. The differences from previous works could relate with the low substrate temperature and relatively high [Se]/[metal] during 3rd stage in our multi stage process. As shown in Fig. 5(a) and (b), a certain influences of Se flux during growth of CIGS layers are observed on the short circuit current density (J_{SC}) and Fill Factor (FF). The increase in the J_{SC} under low [Se]/[Metal] condition attributes to the change in GGI grading shown in Fig. 4.

Figure 6 shows EQE curves of devices with CIGS layers grown under low and high Se condition shown in Fig. 3. As expected from GGI depth grading, a clear shift of the

bandgap is observed, resulting in the increase in the J_{SC} values. In contrast to the behavior of J_{SC} and FF, no clear effects depending on the [Se]/[Metal] ratio are seen for the open circuit voltage (V_{OC}) and efficiency. A simple device simulation using SCAPS suggests that the behavior of the device properties depending on [Se]/[Metal] could be explained by change in the electric properties together with the change in GGI grading (not shown).

3.3. Effect of CIGS thickness

By increasing the deposition rate of all metal constituents, the thickness of CIGS layers was increased to more than 3 μm. For those experiments, the ratio of [Se]/([Cu]+[Ga]), which is the minimum [Se]/[metal] ratio during the preparation processes, was controlled to 4-5. Figure 7 shows J_{SC} (Fig. 7(a)) and efficiency (Fig. 7(b)) of CIGS solar cells with various absorber layer thicknesses. The closed and open circles are the average and best results of cells on one substrate, respectively. It is clearly shown that the J_{SC} and efficiency increase with the thickness up to about 2.8 μm, and the values reach over 35 mA/cm^2 and over 18 % for solar cells (w/o AR coating). EQE curves of devices with CIGS layers with the thicknesses of 2.4 μm and 2.8 μm are shown in Fig. 8. The main difference of EQE curves in Fig. 8 is the response in long wavelength region above 600 nm. Figure 9 shows GGI depth profiles of CIGS films with the thicknesses of 2.4 μm and 2.8 μm. The GGI profiles of CIGS layers grown by multi stage process at substrate temperature <500 °C show a plateau around the GGI minimum (Fig. 4 and 9). This results from co-deposition of Cu and Ga during 2nd stage. As shown in Fig. 9 the width of the plateau around GGI minimum is

expanded from about 240 nm to 400 nm when the film thickness is increased from 2.4 μm to 2.8 μm. The observed improvement in long wavelength region in Fig. 8 would be related to incomplete absorption of light in that region for the 2.4 μm film. Therefore, the widening of the GGI plateau could be the reason for the improved response in long wavelength region, attributing to the increased path length for optical absorption. We believe that there is still room to improve the optical responses of the CIGS solar cell which could be realized by designing the GGI depth profile in combination with a sophisticated light management, such as applied for Si solar cells.

4. Summary

In situ Se flux control system is successively applied for the growth for CIGS absorber layers by the multi stage thermal co-deposition of elements at low substrate temperature below 500 °C. It was revealed that the microstructure of CIGS layers and GGI composition depth profiles changed depending on the [Se]/[Metal] conditions. This suggests that the chemistry and kinetics of CIGS formation reaction and diffusion during 2nd stage is affected by the [Se]/[Metal] ratio. Despite the clear change in the GGI grading, the efficiency of solar cells did not change significantly.

With careful control of [Se]/[Metal] ratio during the preparation process, CIGS layers with various thickness from about 2 μm to over 3 μm were prepared and the devices properties are evaluated. By increasing the thickness from 2.4 μm to 2.8 μm, the J_{SC} is increased from about 33 mA/cm^2 to over 35 mA/cm^2. With increase in the J_{SC}, the

efficiency improves to over 18 %. The increase in J_{SC} is considered to result from the widening of the GGI notch.

Acknowledgments

This work was partially supported by the Swiss Federal Office of Energy under grant agreement SI/501145-01.

References

[1] Solar Frontier Achieves World Record Thin-Film Solar Cell Efficiency: 22.3%, (2015). http://www.solar-frontier.com/eng/news/2015/C051171.html.

[2] Thin-film photovoltaics success story continues, (2016). https://www.zsw-bw.de/en/newsroom/news/news-detail/news/detail/News/thin-film-photovoltaics-success-story-continues.html.

[3] S. Chaisitsak, A. Yamada, M. Konagai, Preferred Orientation Control of Cu(In1-xGax)Se2 (x ≈0.28) Thin Films and Its Influence on Solar Cell Characteristics, Jpn. J. Appl. Phys. 41 (2002) 507–513. doi:10.1143/JJAP.41.507.

[4] G. Hanna, J. Mattheis, V. Laptev, Y. Yamamoto, U. Rau, H.W. Schock, Influence of the selenium flux on the growth of Cu(In,Ga)Se2 thin films, Thin Solid Films. 431–432 (2003) 31–36. doi:10.1016/S0040-6090(03)00242-6.

[5] K. Sakurai, R. Hunger, R. Scheer, C.A. Kaufmann, A. Yamada, T. Baba, Y. Kimura, K. Matsubara, P. Fons, H. Nakanishi, S. Niki, In situ diagnostic methods for thin-film fabrication: utilization of heat radiation and light scattering, Prog. Photovolt. Res. Appl. 12 (2004) 219–234. doi:10.1002/pip.519.

[6] M.A. Contreras, I. Repins, W.K. Metzger, M. Romero, D. Abou-Ras, Se activity and its effect on Cu(In,Ga)Se2 photovoltaic thin films, Phys. Stat. Sol. (a). 206 (2009) 1042–1048. doi:10.1002/pssa.200881243.

[7] S. Ishizuka, A. Yamada, H. Shibata, P. Fons, K. Sakurai, K. Matsubara, S. Niki, Large grain Cu(In,Ga)Se2 thin film growth using a Se-radical beam source, Sol. Energy Mater. Sol. Cells. 93 (2009) 792–796. doi:10.1016/j.solmat.2008.09.043.

[8] T. Sakurai, M.M. Islam, H. Uehigashi, S. Ishizuka, A. Yamada, K. Matsubara, S. Niki, K. Akimoto, Dependence of Se beam pressure on defect states in CIGS-based solar cells, Sol. Energy Mater. Sol. Cells. 95 (2011) 227–230. doi:10.1016/j.solmat.2010.04.036.

[9] S. Ishizuka, A. Yamada, P. Fons, S. Niki, Texture and morphology variations in (In,Ga)2Se3 and Cu(In,Ga)Se2 thin films grown with various Se source conditions, Prog. Photovolt: Res. Appl. 21 (2013) 544–553. doi:10.1002/pip.1227.

[10] M.M. Islam, A. Uedono, T. Sakurai, A. Yamada, S. Ishizuka, K. Matsubara, S. Niki, K. Akimoto, Impact of Se flux on the defect formation in polycrystalline Cu(In,Ga)Se2 thin films grown by three stage evaporation process, J. Appl. Phys. 113 (2013) 64907-64907–7. doi:10.1063/1.4792049.

[11] S. Nishiwaki, F. Pianezzi, B. Bissig, P. Reinhard, S. Buecheler, H. Schuler, C. Eisele, A.N. Tiwari, Precise Control of Se Flux for High Quality Cu(In,Ga)Se2 Absorber Layer Deposition at Low Substrate Temperature by UV Light Absorption in Vapor Phase, in: WCPEC-6 Technical Digest, Kyoto, 2014: p. 3WePo.6.5.

[12] A. Chirilă, S. Buecheler, F. Pianezzi, P. Bloesch, C. Gretener, A.R. Uhl, C. Fella, L. Kranz, J. Perrenoud, S. Seyrling, R. Verma, S. Nishiwaki, Y.E. Romanyuk, G. Bilger, A.N. Tiwari, Highly efficient Cu(In,Ga)Se2 solar cells grown on flexible polymer films, Nat Mater. 10 (2011) 857–861. doi:10.1038/nmat3122.

[13] S.C. Jackson, B.N. Baron, R.E. Rocheleau, T.W.F. Russell, A chemical reaction model for physical vapor deposition of compound semiconductor films, AIChE J. 33 (1987) 711–721. doi:10.1002/aic.690330503.

[14] L. Roussak, G. Wagner, L. Makhova, I. Konovalov, Epitaxial CuIn1-xGaxSe2/ZnS heterostructures grown on (001)GaAs by co-evaporation, Phys. Status Solidi C. 6 (2009) 1287–1290. doi:10.1002/pssc.200881209.

[15] A.M. Gabor, J.R. Tuttle, D.S. Albin, M.A. Contreras, R. Noufi, A.M. Hermann, High-efficiency CuInxGa1-xSe2 solar cells made from (Inx,Ga1-x)2Se3 precursor films, Appl. Phys. Lett. 65 (1994) 198–200.

[16] N. Kohara, T. Negami, M. Nishitani, T. Wada, Preparation of Device-Quality Cu(In, Ga)Se2 Thin Films Deposited by Coevaporation with Composition Monitor, Jpn. J. Appl. Phys. 34 (1995) L1141-K1144.

[17] A.M. Gabor, J.R. Tuttle, M.H. Bode, A. Franz, A.L. Tennant, M.A. Contreras, R. Noufi, D.G. Jensen, A.M. Hermann, Band-gap engineering in Cu(In,Ga) Se2 thin films grown from (In,Ga)2Se3 precursors, Sol. Energy Mater. Sol. Cells. 41–42 (1996) 247–260. doi:10.1016/0927-0248(95)00122-0.

[18] H. Rodriguez-Alvarez, R. Mainz, S. Sadewasser, A one-dimensional Fickian model to predict the Ga depth profiles in three-stage Cu(In,Ga)Se2, J. Appl. Phys. 115 (2014) 204913. doi:10.1063/1.4880298.

[19] D.J. Schroeder, G.D. Berry, A.A. Rockett, Gallium diffusion and diffusivity in CuInSe[sub 2] epitaxial layers, Appl. Phys. Lett. 69 (1996) 4068–4070.

Figure captions

Fig. 1 Relative fluxes of Cu, In, Ga, and Se and substrate temperature during deposition process. The relative flux ratios between Cu, In, and Ga are kept constant through this work.

Fig. 2 Substrate heater power around stoichiometry point under typical and low [Se]/[Metal] conditions. Arrowed points are the stoichiometry point calculated from the film compositions analyzed by XRF.

Fig. 3 Cross-section SEM images of CIGS layers grown under (a) low, (b) middle, and (c) high [Se]/[Metal] conditions. The conditions (a), (b), and (c) correspond to [Se]/([Cu]+[Ga])=2.5, 4.1 and 7.5, respectively.

Fig. 4 GGI composition depth profiles of CIGS layers grown under low and high [Se]/[Metal] conditions corresponding to Fig. 3.

Fig. 5 Solar cell properties of devices with CIGS layer grown under various [Se]/[Metal] conditions: (a) short circuit current density, (b) fill factor, (c) open circuit voltage, (d) efficiency. Closed circles indicate the average from devices on one substrate (18 cells × ~0.57 cm^2), and the error bars indicate the maximum and minimum. The dotted lines indicate the functional low limit of the end point detection.

Fig. 6 External quantum efficiency of solar cell devices with CIGS layer grown under low and high [Se]/[metal] conditions shown in Fig. 3 and 4.

Fig. 7 CIGS thickness dependence of (a) J_{SC} and (b) Efficiency. Closed and open circles indicate the averages and the best results on one substrate, respectively. All layers

were prepared according to the process shown in Fig. 1 controlling [Se]/([Cu]+[Ga]) ratios to 4-5. Subsequently, sodium fluoride post deposition treatment was applied.

Fig. 8 External quantum efficiency curves from devices of CIGS layers with a thickness of 2.4 μm and 2.8 μm. During the preparation, the ratios of [Se]/([Cu]+[Ga]) were controlled to 4.1 and 4.4 for the sample with 2.4 μm and 2.8 μm thick, respectively.

Fig. 9 GGI composition depth profiles of CIGS layers with different thicknesses shown in Fig. 8.

Fig. 1

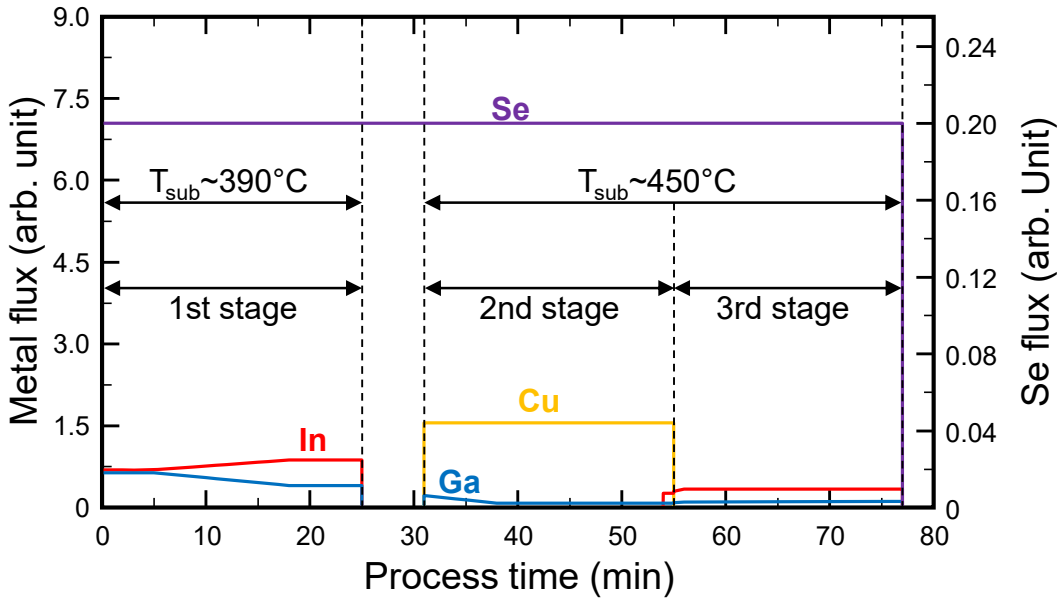
Metal flux (arb. unit)
Se flux (arb. Unit)
Process time (min)
Se
T_{sub}~390°C
T_{sub}~450°C
1st stage
2nd stage
3rd stage
Cu
In
Ga
9.0
7.5
6.0
4.5
3.0
1.5
0
0.24
0.20
0.16
0.12
0.08
0.04
0
0
10
20
30
40
50
60
70
80

Fig. 2

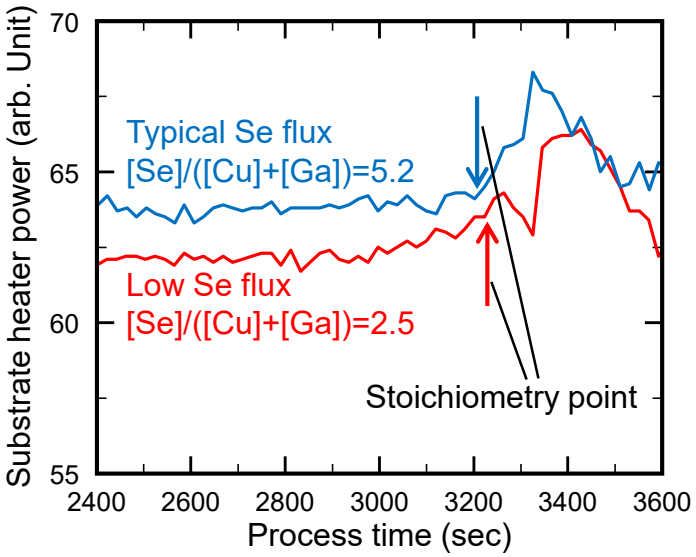
Substrate heater power (arb. Unit)
Process time (sec)
Typical Se flux
[Se]/([Cu]+[Ga])=5.2
Low Se flux
[Se]/([Cu]+[Ga])=2.5
Stoichiometry point
70
65
60
55
2400
2600
2800
3000
3200
3400
3600

Fig. 3

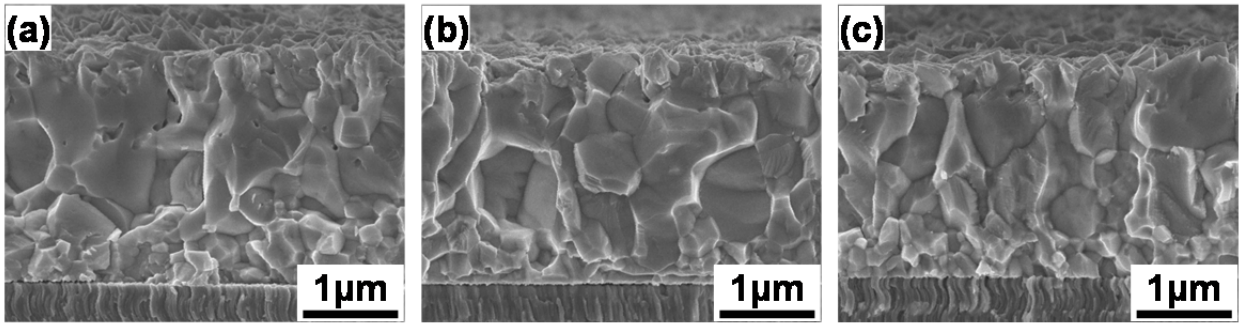
(a)
1μm
(b)
1μm
(c)
1μm

Fig. 4

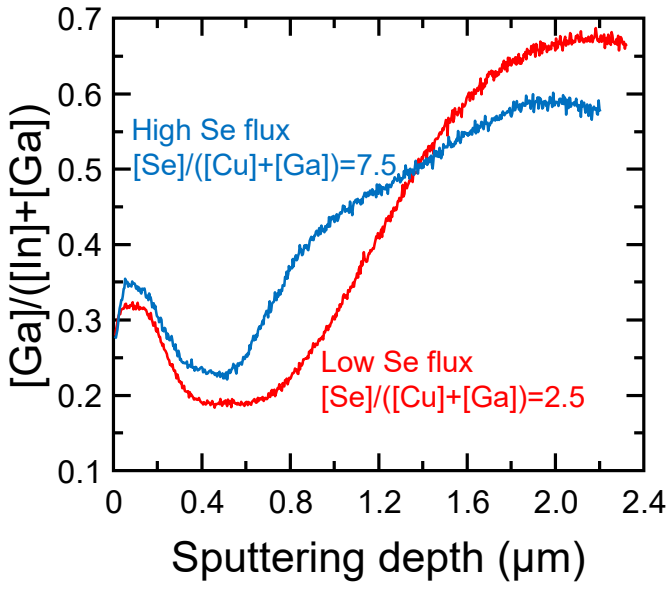
0.7
0.6
0.5
0.4
0.3
0.2
0.1
[Ga]/([In]+[Ga])
High Se flux
[Se]/([Cu]+[Ga])=7.5
Low Se flux
[Se]/([Cu]+[Ga])=2.5
0
0.4
0.8
1.2
1.6
2.0
2.4
Sputtering depth (μm)

Fig. 5

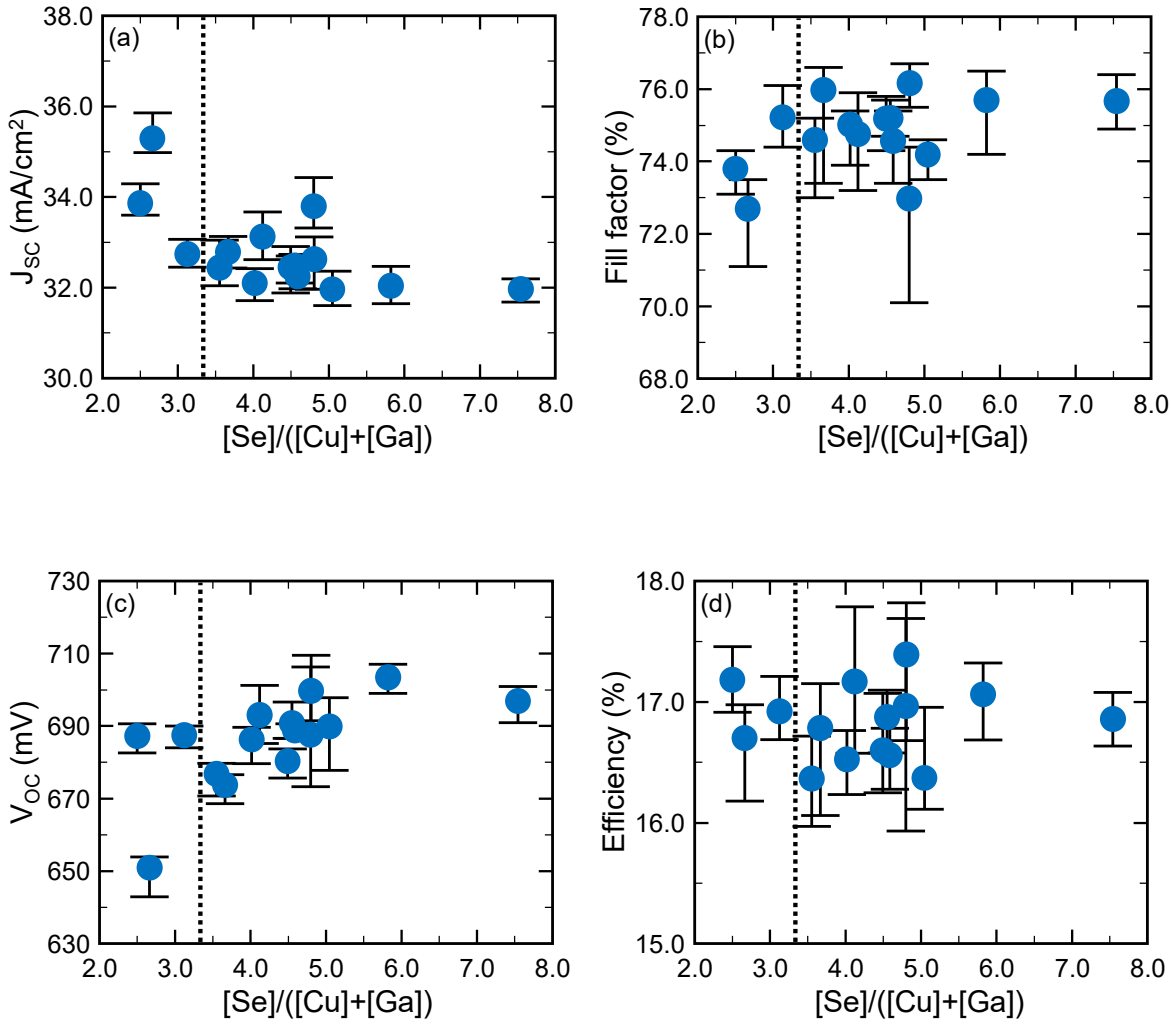
(a)
J_{SC} (mA/cm^2)
38.0
36.0
34.0
32.0
30.0
2.0
3.0
4.0
5.0
6.0
7.0
8.0
[Se]/([Cu]+[Ga])
(b)
Fill factor (%)
78.0
76.0
74.0
72.0
70.0
68.0
[Se]/([Cu]+[Ga])
(c)
V_{OC} (mV)
730
710
690
670
650
630
[Se]/([Cu]+[Ga])
(d)
Efficiency (%)
18.0
17.0
16.0
15.0
[Se]/([Cu]+[Ga])

Fig. 6

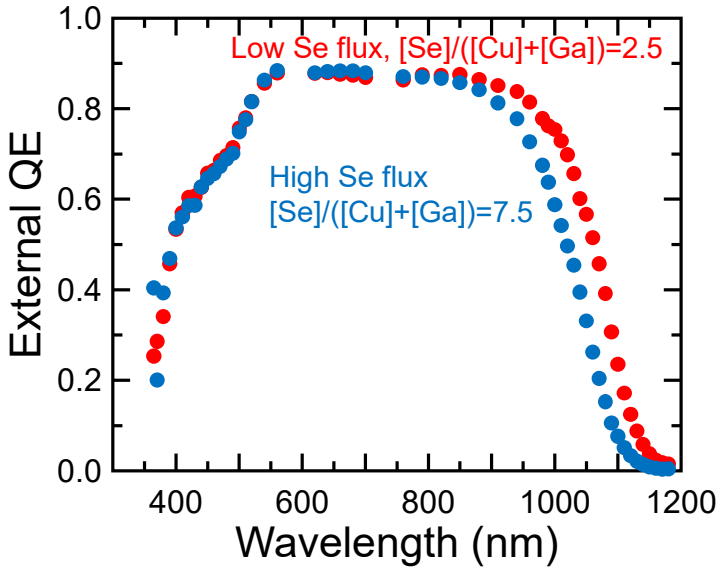
Low Se flux, [Se]/([Cu]+[Ga])=2.5
High Se flux
[Se]/([Cu]+[Ga])=7.5
External QE
1.0
0.8
0.6
0.4
0.2
0.0
400
600
800
1000
1200
Wavelength (nm)

Fig. 7

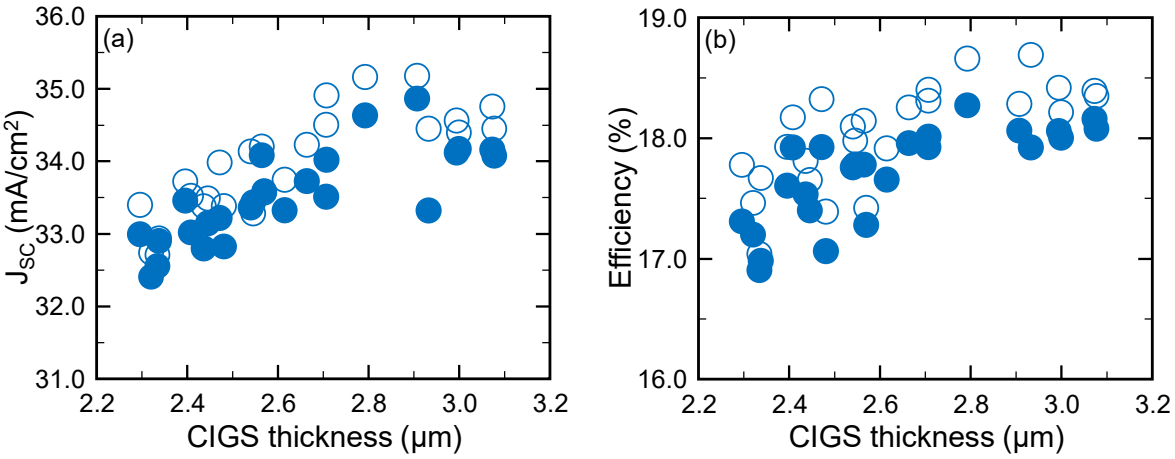
(a)
J_{SC} (mA/cm^2)
36.0
35.0
34.0
33.0
32.0
31.0
2.2
2.4
2.6
2.8
3.0
3.2
CIGS thickness (μm)
(b)
Efficiency (%)
19.0
18.0
17.0
16.0
2.2
2.4
2.6
2.8
3.0
3.2
CIGS thickness (μm)

Fig. 8

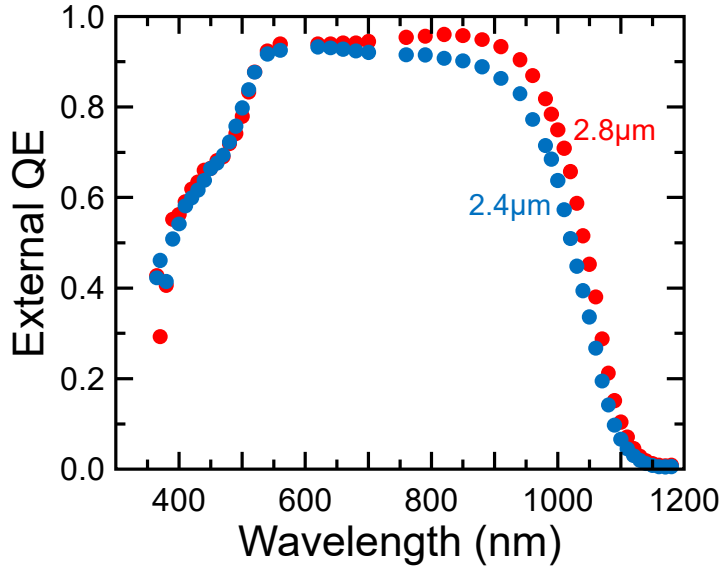
External QE
1.0
0.8
0.6
0.4
0.2
0.0
400
600
800
1000
1200
Wavelength (nm)
2.8μm
2.4μm

Fig. 9

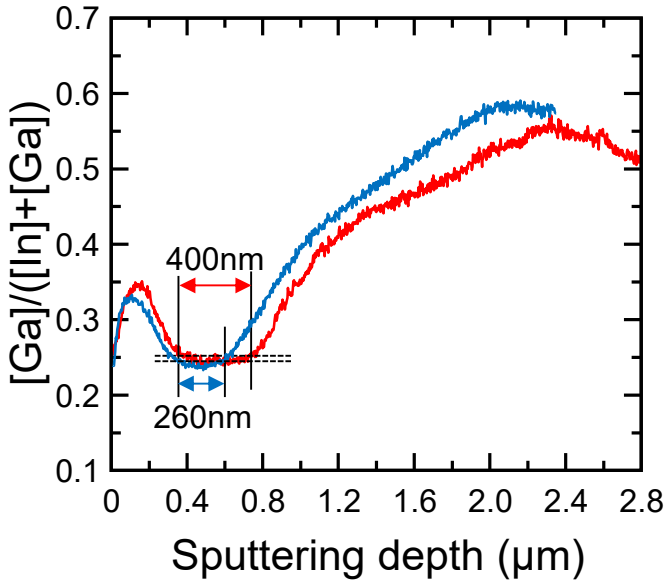
0.7
0.6
0.5
0.4
0.3
0.2
0.1
[Ga]/([In]+[Ga])
400nm
260nm
0
0.4
0.8
1.2
1.6
2.0
2.4
2.8
Sputtering depth (μm)